Global and Planetary Change 172 (2019) 256–267

Contents lists available at ScienceDirect

Global and Planetary Change

journal homepage: www.elsevier.com/locate/gloplacha

Wave refraction and reef island stability under rising sea level

Mirella B. Costa[a,*,1], Eduardo C. Macedo[b], Eduardo Siegle[a]

[a] Instituto Oceanográfico, Universidade de São Paulo, Praça do Oceanográfico, 191, 05508-120 Sao Paulo, SP, Brazil
[b] Rebio Atol das Rocas, Instituto Chico Mendes de Conservação da Biodiversidade, Av. Alexandrino de Alencar, 1399, 59015-350 Natal, RN, Brazil

ARTICLE INFO

Keywords:
Wave convergence
Reef island migration
Climate change
South Atlantic Ocean
Rocas Atoll

ABSTRACT

The location and stability of low-lying carbonated reef islands are closely related to wave refraction over reef platforms, which create low energy wave convergence zones favorable for sediment deposition. Although there is great concern about the stability of reef islands in future decades, few studies have attempted to assess the effects of sea-level rise on wave refraction patterns and the migration of wave convergence zones, which may promote changes in island positions. To investigate the mechanisms of wave refraction over a shallow lagoon atoll (Rocas Atoll), we performed a detailed topo-bathymetric survey to simulate wave propagation for different water levels and wave conditions considering the complex atoll morphology. Our results show that the locations of convergence zones are not only influenced by wave direction and wave interactions with the elliptical reef shape but also controlled by topographic variations in the reef structure. In particular, the presence of a wide reef passage on the leeward margin of Rocas Atoll has an important role in the atoll wave refraction pattern. Model simulations show a displacement of the wave convergence zone and increase in wave energy under increased sea level. However, the direction of this displacement is more sensitive to the incident wave period than to the wave direction due to topographic control. Swell waves, either from the north or south, tend to move the convergence zone lagoonwards, whereas wind waves tend to move this zone seawards. Thus, the results suggest that, under sea-level rise scenarios, areas prone to sediment accumulation will become less stable. The relative frequency between swell and wind wave incidence will be an important driver of morphological change patterns in reef islands.

1. Introduction

Wave refraction provides a major driving mechanism for reef-top hydrodynamics, which subsequently control the entrainment and transfer of sediment to depositional centers on the reef flat (Gourlay, 1988; Mandlier and Kench, 2012). Open ocean swell is filtered at the reef crest, but a component of the wave energy crosses the reef flat and reaches the island shore (Woodroffe and Biribo, 2011). Reef structures promote the refraction and diffraction of this residual wave energy and critically influence the propagation behavior of waves across reef surfaces (Mandlier and Kench, 2012). As a consequence, such wave processes create low energy wave convergence zones (or nodal zones) favorable for sediment deposition and reef island formation (Flood, 1986; Gourlay, 1988; Kench and Brander, 2006).

Studies focusing on three-dimensional approaches to wave transformations have demonstrated that the location and stability of low-lying carbonated reef islands are closely related to nodal zones on reef platforms (Flood, 1986; Gourlay, 1988; Kench and Brander, 2006; Mandlier, 2013; Mandlier and Kench, 2012). For example, changes in the direction of the incident wave can produce a change in the position of the nodal point and a reorientation of reef island shorelines (Flood, 1986). Thereby, seasonal variations in reef island morphology are expected to occur in response to seasonal variations in wave characteristics (Kench et al., 2009a, 2009b), showing the inherent sensitivity of reef islands to changes in boundary conditions.

Due to the dynamic nature of reef islands and their typically low elevations (< 3 m above mean sea level), there is significant global concern over the physical vulnerability of these islands in response to climatic changes including sea-level rise and increased storminess (McKoy et al., 2010). Recent observations have shown that the rate of global mean sea-level rise during the 21st century will exceed the 1971–2010 rate for all representative concentration path-way (RCP) scenarios (Church et al., 2013), reinforcing the urgent need to assess the vulnerability of reef islands to this aspect of climate change (Woodroffe,

* Corresponding author.
E-mail address: mirella.costa@ufpe.br (M.B. Costa).
[1] Now at Departamento de Oceanografia, Universidade Federal de Pernambuco, Av. Arquitetura s/n, Cidade Universitária, Recife, Pernambuco, CEP: 50670–901, Brazil.

https://doi.org/10.1016/j.gloplacha.2018.10.015
Received 26 July 2018; Received in revised form 14 October 2018; Accepted 19 October 2018
Available online 21 October 2018
0921-8181/ © 2018 Elsevier B.V. All rights reserved.

2008). Much of the concern about accelerating sea-level rise centers on the question of whether reef islands on atolls will be lost via erosion and flooding in future decades (Forbes et al., 2013).

One of the effects of sea-level rise is the creation of deeper waters over reefs and lagoons, potentially allowing larger waves to reach reef island shorelines (Baldock et al., 2014) or reef coasts (Siegle and Costa, 2017). Storlazzi et al. (2015) show that waves will synergistically interact with sea-level rise, doubling the forecast of land flooding for a given value of sea-level rise when wave-driven water level is accounted. On the other hand, studies have also shown that reef islands are morphologically resilient landforms that can increase in area despite sea-level rise (Duvat et al., 2017) and that island erosion should be considered as one of a spectrum of possible geomorphic changes (Webb and Kench, 2010). Using analytical models, Mandlier and Kench (2012) demonstrated that changes in water depth (a surrogate for increased sea level) and wave period may promote change in island position on reef surfaces due to the migration of wave convergence points.

Despite the overall recognition of the importance of planform wave processes on reef island stability, few studies have attempted to assess the effects of sea-level rise on refraction patterns over reef surfaces. Third-generation wave models numerically solved the wave action conservation equations (Booij et al., 1999; Sorensen et al., 2004), which include depth-induced wave processes such as refraction, shoaling, dissipation by bottom friction and breaking. These models have been extensively used for wave propagation research in coastal regions (Allard et al., 2008; Dan et al., 2011; Pattiaratchi et al., 2009; Stone et al., 2005), including applications in coral reef environments (Baldock et al., 2014; Filipot and Cheung, 2012; Golshani et al., 2012; Hoeke and Storlazzi, 2013; Hoeke et al., 2011; Lowe et al., 2010; Storlazzi et al., 2011; Vitousek et al., 2007) and atolls (Hoeke, 2010; Sato and Yokoki, 2010; Storlazzi et al., 2015). One of the advantages to using numerical models is the ability to create hypothetical scenarios to evaluate changes in sea level and wave characteristics according to modifications in boundary conditions for complex topographies.

With a combination of in situ data and numerical modeling, this paper aims to study the refraction patterns and wave energy distribution in a small and shallow lagoon. Rocas is the only atoll in the South Atlantic Ocean and is a pristine and uninhabited marine protected area. Despite its small size, Rocas is an important sanctuary for thousands of seabirds, green turtles and an endemic land crab that relies on Rocas reef islands. Due to the absence of man-made structures, except for one small research station, Rocas serves as a laboratory to study natural processes without direct human interference. To reproduce the effects of local morphological features, such as reef passages and sand aprons, on wave refraction, a detailed description of the topo-bathymetry of the Rocas atoll is included in the present work and used as input to the numerical model. The wave propagations under current conditions and a sea-level rise scenario are compared, and the reef island stability implications of this comparison are discussed.

1.1. Study site

Rocas Atoll (3.863° S, 33.804° W) is a small and shallow lagoon atoll located in the western portion of a South Atlantic seamount with surrounding waters with an average depth of 25 m and a shelf-break depth of approximately 50 m (Fig. 1). The atoll lagoon has an average depth of 3 m and is filled by a large sand apron that covers almost half of the lagoon and emerges during low tides (Costa et al., 2017b). A maximum depth of 7 m is found near the larger reef passage, which is 300 m wide and 500 m long (Costa et al., 2017b). The smaller reef passage is separated from the lagoon during the low and intermediary tides by sand aprons that connect both reef islands (Farol and Cemitério). This smaller passage has an average depth of 3 m and is 30 m in length and 70 m in width.

The region experiences a semidiurnal mesotidal regime with a spring and neap tidal range of 2.8 m and 1.7 m, respectively (Costa et al., 2017b). Southeast trade winds prevail during 93% of the year (BDC, 2015), varying in strength according to the Intertropical Convergence Zone (ITCZ) seasonality (McGregor and Nieuwolt, 1998). The average wind speed is approximately 5 m/s, with a maximum speed of approximately 11 m/s (BDC, 2015). As a result, south wind waves with significant wave heights from 0.5 to 2.5 m dominate the wave field at Rocas and break on the windward reef crest during most of the year (Costa et al., 2017b). In turn, waves breaking on the windward reef rim drive the lagoon circulation, causing a consistent westward flow through the atoll and outflow though the reef passages (Costa et al., 2017b). During low tides, the wave pumping mechanism is blocked by the vertical exposure of the reef rim, causing flow reversal at the large reef passage (Costa et al., 2017b). Due to its location near the Equator, north- and southward-directed swells, which are generated during the winters of both hemispheres, also contribute to the wave conditions of Rocas (Costa et al., 2017b). Significant wave heights in the lagoon range from 0.01 to 0.81 m, with maximum values during high spring tides. The lagoon wave spectrum is dominated by both infragravity wave energy (> 0.05 Hz) and wind wave energy (0.333–0.125 Hz) (Costa et al., 2017b).

The reef islands are on the leeward reef rim separated by the smaller reef passage. The reef flat on which they are located is approximately 1.5 m from the mean low spring water (MLSW). The MLSW corresponds to the vertical datum where the reef flat is totally exposed and the lagoon water volume is restricted near the larger reef passage entrance (perennial lagoon). The vegetated island surface ranges from 2 m to 3.7 m above the reef flat surface and from 3.5 m to 5.2 m above the MLWS. The two islands have different planform morphologies. Farol is horseshoe shaped, with a series of asymmetric low-elevation ridges and a central depression. The oceanward ridge is higher than the lagoonward ridge by approximately 1.7 m. Cemitério Island has an elongated planform shape with a flat top, marked by a slight difference of 0.5 m between the oceanward (5 m above MLWS) and lagoonward edge (4.5 m above MLWS). The Zulu shingle bank is located on the windward reef flat 1.1 m above MLWS. This bank has an elongated shape with a top that reaches up to 2.4 m above MLWS. A detailed description of the reef islands and the shingle bank morphology is presented in Costa et al. (2017a). The reef islands are predominantly composed of coarse-grained sand, the shingle bank is composed of gravel and the sand apron is composed of medium-grained sand (Pereira et al., 2013). The sediments are composed entirely of carbonate skeleton derived from the reef system (Pereira et al., 2013).

Despite the small sizes of the reef islands, they contain abundant fauna comprising visiting or nesting birds. The islands shelter the largest breeding colonies of masked booby (*Sula dactylatra*) and brown noddy (*Anous stolidus*) in Brazil and the largest breeding colony of sooty tern (*Sterna fuscata*) in the South Atlantic (Schulz-Neto, 2004). Rocas Atoll is also the second largest *Chelonia mydas* rookery in Brazil (Bellini et al., 1996) and an important place for the protection of an endemic species of land crab (*Johngarthia lagostoma*) that only occurs on three other South Atlantic islands (Trindade, Fernando de Noronha and Ascension) (Godley et al., 2009).

2. Methods

2.1. Topographic and bathymetric surveys

To represent the complex topography of the atoll, topographic surveys were conducted using a dual-frequency kinematic Global Position System (GPS). The instrument consisted of two GPS receivers, one serving as a base station (Trimble 5700) that remained at a fixed position throughout each of the surveys, and the other serving as a rover unit (Trimble R4) taken to individual measurement points. A geodetic benchmark (survey mark) on Farol Island was used as the reference point for the base station. Surveys at the exposed parts of the atoll, such as the reef rim and the reef islands, were conducted by foot

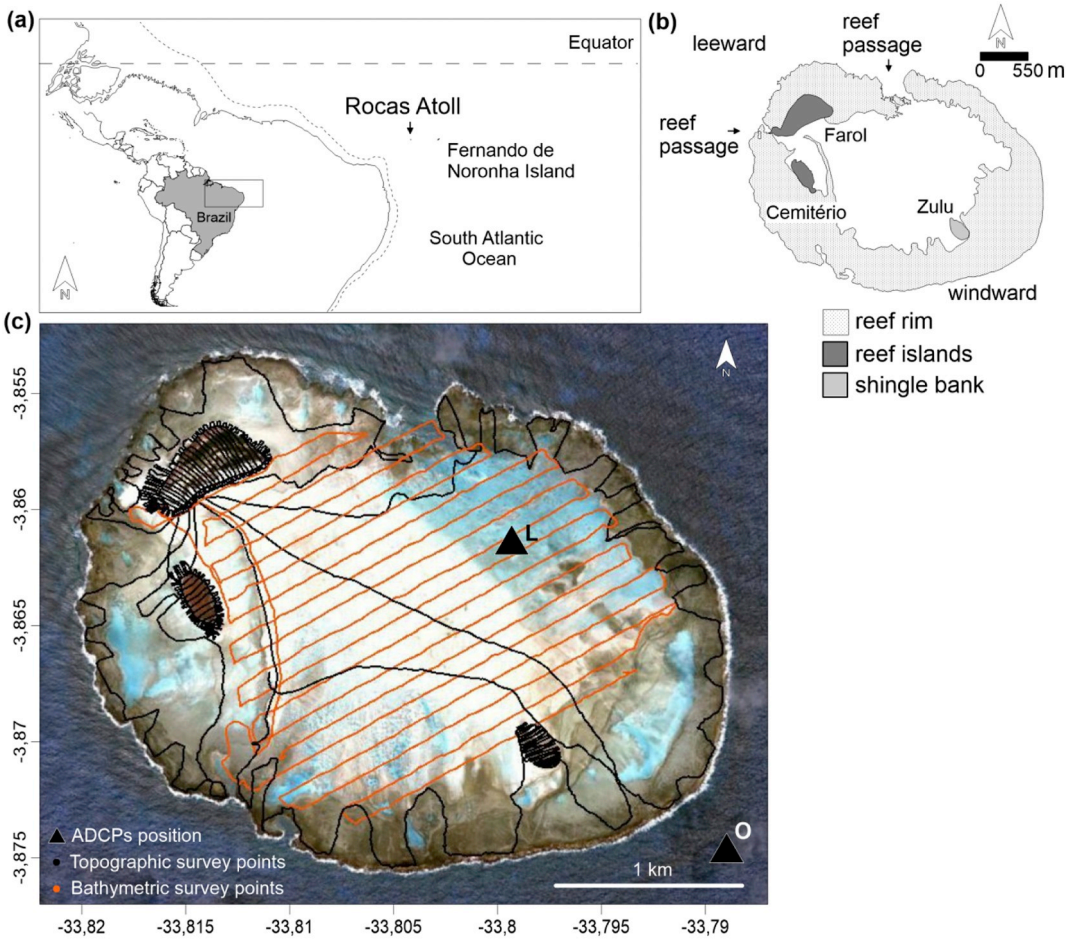

Fig. 1. (a) Location of Rocas Atoll. (b) Description of Rocas Atoll. (c) Bathymetric and topographic survey points for the lagoon, reef islands, shingle bank and reef rim. Black lines represent the survey track for the dry parts of the atoll; these surveys were conducted using the rover in a backpack kit during low tides. Orange lines represent the survey track for the lagoon and sand apron; these surveys were conducted using the rover coupled to an echosound on a monohull vessel during high tides. Black triangles represent the lagoon and offshore ADCP positions.

during low tides using the rover GPS equipment mounted in a backpack kit. The lagoon was surveyed by coupling the rover unit with a Garmin echosounder installed in a monohull vessel. The measurements were done along equally spaced profiles (100 m) during high tides. The GPS surveys were carried out as post-processed kinematic surveys (PPK GPS), where positional data from the roving GPS were processed with the help of data from the stationary base GPS using TBC software (horizontal and vertical accuracy of ± 20 mm) (Fig. 1). The bathymetry of the offshore waters was gathered from Brazilian Navy nautical charts, specifically charts 5101 and 5102. The in situ surveyed data were tidally corrected, and the vertical datum of each source (in situ and nautical charts) was adjusted to the Rocas Atoll MLWS provided by the Brazilian Navy.

2.2. Numerical wave model

A numerical wave propagation model (MIKE21 SW) was implemented on Rocas Atoll to simulate incoming waves over the atoll's complex bathymetry. MIKE21 SW represents a third-generation spectral wave model that solves the wave action conservation equation using a parameterization of the zeroth and first-order moments of the wave action spectrum in the frequency domain (Holthuijsen et al., 1989). The model estimates the transformation of incident wave energy by shoaling, refraction, diffraction, and dissipation by both depth-induced wave breaking and bottom friction (Sorensen et al., 2004).

An unstructured nested mesh with three different resolutions was created to solve the differences in the bathymetric scale along the model domain. The finer grid encompassing the atoll topography and the surrounding waters shallower than 20 m, were refined to approximately 20 m spatial resolution. The high resolution in situ surveyed topo-bathymetric data were used to represent the complex topography of the atoll. Bathymetric data of the offshore deep waters (> 3000 m) and the waters over the insular shelf (20 m to 70 m) were gathered from nautical charts and represented by a coarser grid.

A constant breaker coefficient of $\gamma = 0.8$ was used to parameterize the wave breaking-induced dissipation. The gamma value controls the wave steepness conditions, that is, a threshold ratio is reached before the break, considering the local depth. Its formulation is reported in Battjes and Janssen (1978). Wave dissipation due to bottom friction was based on the formulation by Madsen et al. (1988) using a constant Nikuradse bed roughness length of Kn = 0.04 m. This value is equivalent to a friction factor (fw) of 0.1 for smooth healthy coral reefs (Sheppard et al., 2005).

The numerical model was calibrated by comparing the modeled results with data measured in situ by two Acoustic Doppler Current Profilers (ADCPs) deployed for 28 days at Rocas Atoll. The ADCPs operated intermittently with a sampling frequency of 2 Hz. The wave characteristics were measured in 2048 bursts (17.1 min) hourly. One ADCP was deployed in the lagoon at approximately 2 m of depth, whereas the other was deployed outside the atoll at approximately 16 m of depth (Fig. 2).

The calibration process included variations in the parameters

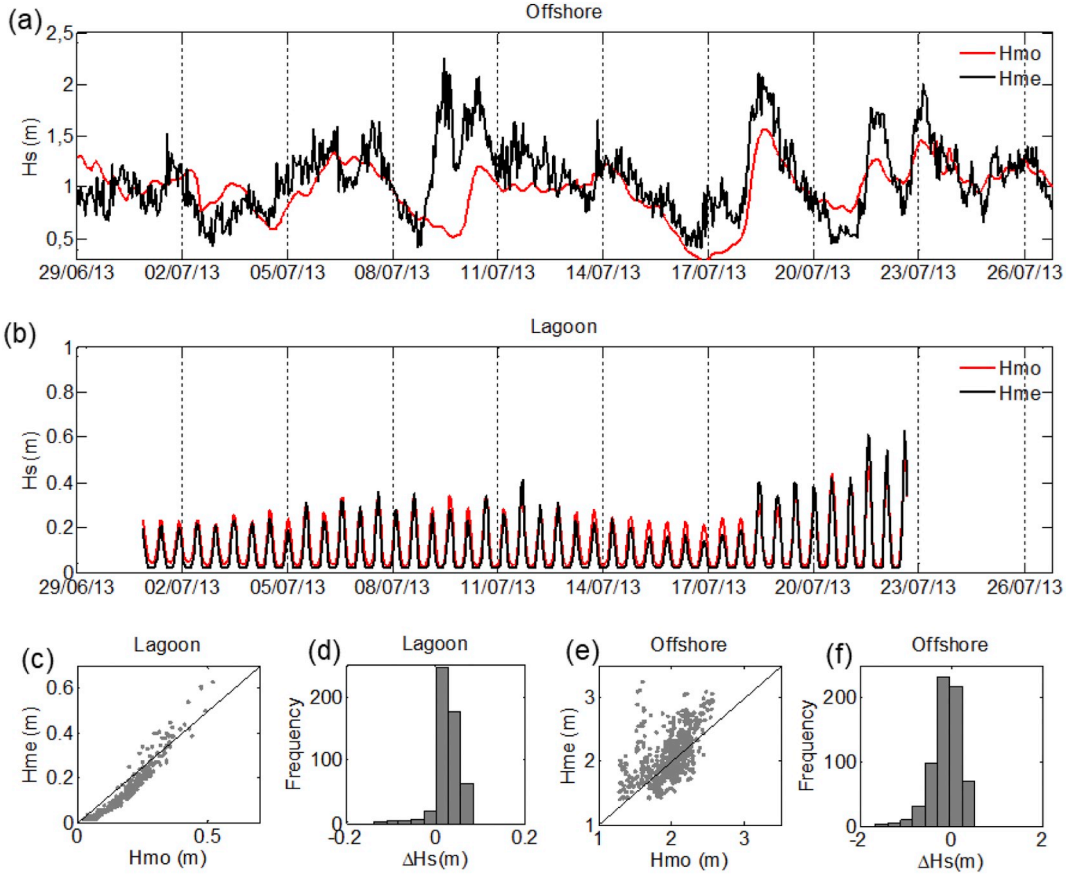

Fig. 2. Time series of the measured (Hme) and modeled (Hmo) significant wave heights used for validation at the (a) offshore and (b) lagoon station. Histogram of model errors and (d,f) scatter diagram of modeled (Hmo) and measured (Hme) significant wave heights for (c,e) the lagoon and offshore stations.

described in the previous section (i.e., mesh resolution, wave breaking parameter, bottom friction) to find the best balance between model computational effort and agreement with the in situ data. The difference between the modeled significant wave height (Hmo) and the measured significant wave height (Hme), mean difference (bias), root-mean-square error (RMSE), and correlation coefficient (cc) for the ADCP match points were used to verify the performance of the model. The model well reproduced the wave conditions both offshore and inside the lagoon. The validation results indicated that the biases of the offshore and lagoon stations were 0.106 m and 0.027 m, respectively, and that the RMSEs were 0.327 m and 0.040 m, respectively. The correlation coefficient (cc) values between Hmo and Hme for the offshore and lagoon stations were 0.507 and 0.964, respectively. The values indicate better model performance in the lagoon than in the offshore region. Tidal modulation of the waves inside the lagoon was observed, with greater heights at high tide and smaller heights at low tide, and this process was well resolved by the model.

The offshore wave characteristics used as boundary inputs to force the wave model were based on the global wave generation model WaveWatch III (NOAA) wave climate analysis for Rocas Atoll. Table 1 contains a summary of the dominant wave conditions used to force the wave model. They represent southeastern trade wind waves and northern and southern swell conditions at Rocas Atoll. These three wave conditions were simulated for the present sea level (scenario SLR = 0) and for 1 m of sea-level rise (scenario SLR = 1), which is close to the RCP8.5 high emission scenario of 0.98 m relative sea-level rise estimated by the IPCC AR5 for 2100 (Church et al., 2013). A total of six numerical experiments were defined to obtain wave parameters for different sea-level scenarios (0 and 1 m) during a full tide cycle, resulting in 22 h of run simulations. For increased sea-level scenarios, 1 m has been added to the mean sea level.

Table 1
Summary of the offshore dominant wave conditions at Rocas Atoll used to construct the wave propagation scenarios.

Scenarios	Incident wave condition	Hs (m)	Tp (s)	Dir (deg)
Scenario 1				
SLR = 0	Northern swell	2	14	0
SLR = 0	Southern swell	2	14	180
SLR = 0	Southeastern wind wave	2	8	135
Scenario 2				
SLR = 1	Northern swell	2	14	0
SLR = 1	Southern swell	2	14	180
SLR = 1	Southeastern wind wave	2	8	135

Model outputs of significant wave height (Hs) and peak wave period (Tp) from the finer grid were used to calculate the wave power (P) distribution over the atoll using the expression:

$$P = \frac{\rho g^2 H_s^2 T_p}{32\pi} \quad (1)$$

where ρ is the water density (1027 kg/m^3) and g is the gravitational acceleration. From Eq. (1), it is possible to quantify the synergy of the wave height and period, providing an estimation of wave dissipation over the atoll. Comparisons of the directional wave vectors were used to assess the wave refraction changes in each scenario.

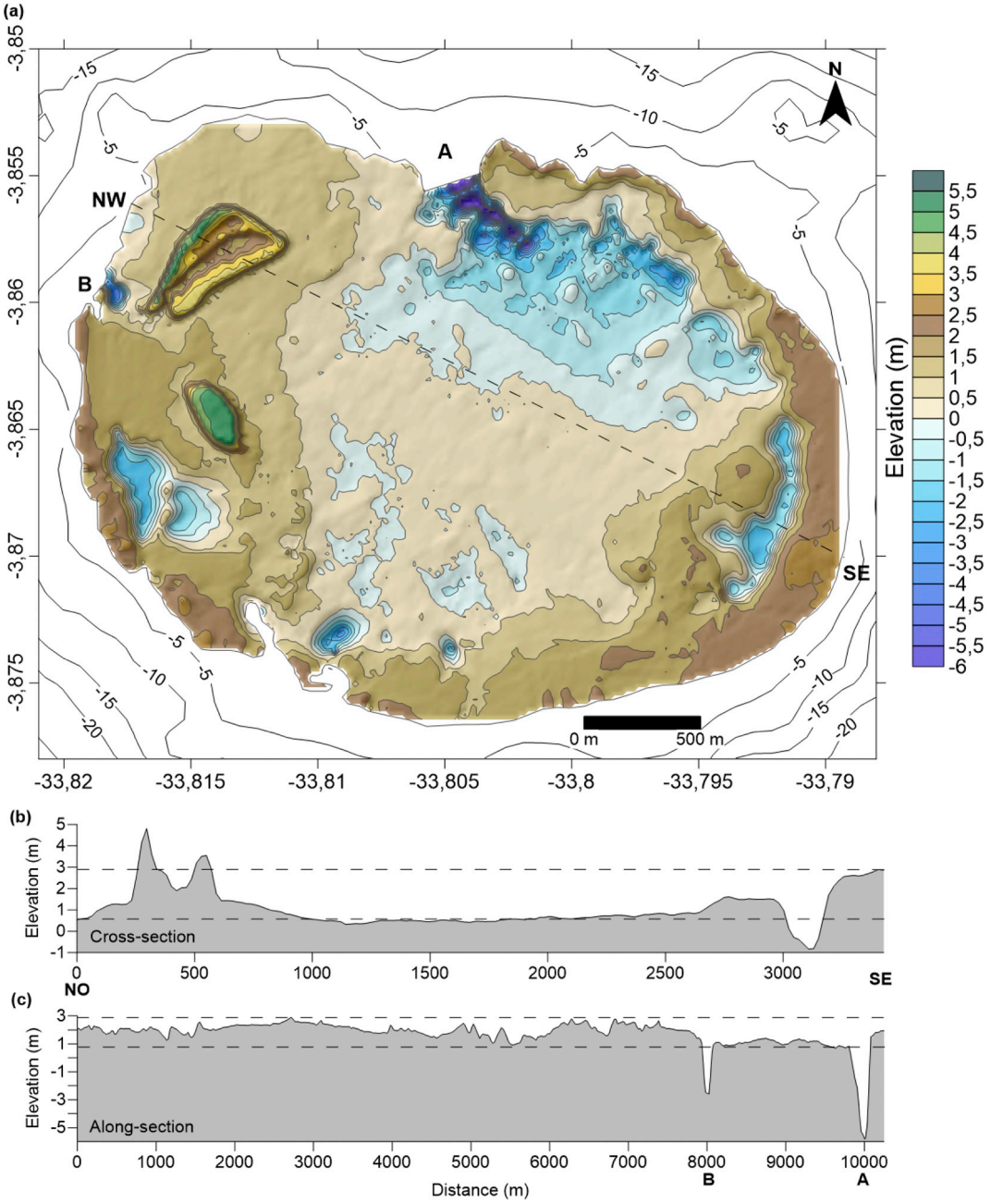

Fig. 3. (a) Digital elevation model of Rocas Atoll. (b) Profile section from the leeward side (NW) to the windward side (SE). (c) reef-crest perimeter profile; the letter A corresponds to the larger reef passage and B corresponds to the smaller passage. Note: the reef boulders and the submerged depressions on the reef rim were not detailed in the survey.

3. Results

3.1. Atoll topography

The surveyed morphology of Rocas Atoll is shown in Fig. 3. The highest point of the atoll is 5.2 m above MLWS, located in the northwest side of Farol Island. The deepest point is 7.8 m below MLWS, located in the larger passage. The entire atoll is flooded during spring high tide, except for Farol and Cemitério Islands and some reef boulders located in the windward portion of the atoll.

The atoll reef rim is noticeably not topographically uniform, with a difference of up to 2.1 m between the windward and leeward sides. The northwestern portion (leeward), between the two reef passages is lower than the rest of the atoll. The mean height of the reef flat in this section is 1.3 m, whereas the remainder of the rim is approximately 2.5 m high. The highest point of the reef rim is located on the southeastern side (windward) and is 2.9 m high. Hundreds of reef boulders of varying sizes are exclusively found on the windward side and numerous submerged depressions (e.g., small pools) are spread across the reef rim. The largest boulder is approximately 6 m high.

3.2. Modeled wave refraction

3.2.1. Present conditions (SLR = 0)

Wave power across the atoll ranges between 0 and 25.8 kW/m for the SLR = 0 scenario. The wave power in the lagoon is at least two orders of magnitude lower than that in the offshore region for any incident wave. At the reef edge, where wave dissipation starts, the wave

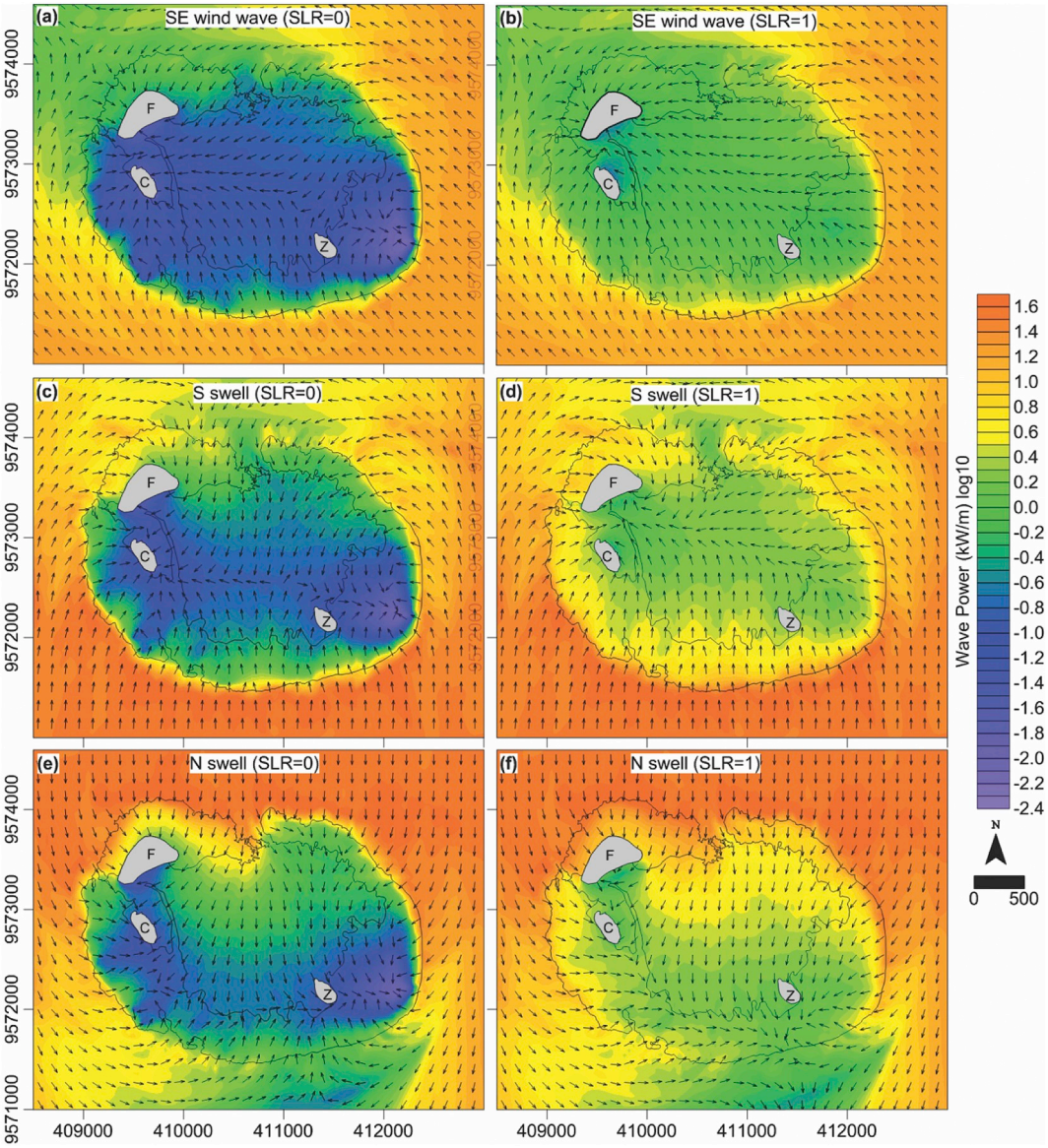

Fig. 4. Distribution of wave power P (kW/m) in Rocas Atoll for southeast wind wave conditions in (a) SLR = 0 and (b) SLR = 1; for south swell wave conditions in (c) SLR = 0 and (d) SLR = 1; and for north swell wave conditions in (e) SLR = 0 and (f) SLR = 1. Data are presented in the logarithmic scale to show details of the P distribution in shallow waters. Linear values of P are displayed beside the logarithmic scale. Letters on the map correspond to the Farol Island (F), Cemitério Island (C) and Zulu shingle bank (Z) locations. Wave vectors are not scaled.

power is one order of magnitude lower than that offshore (Fig. 4a, c, e).

The distribution of wave vectors demonstrates that the atoll wave refraction pattern is highly affected by the larger reef passage (Fig. 4a, c, e). Although this passage is oriented northwards (leeward side), which provides favorable conditions for the penetration of northern swells into the atoll lagoon, both southern and southeastern offshore waves refracted around the reef rim and penetrated through this passage into the lagoon. As a result, the highest values of wave power are found near this entrance and at the leeward reef rim in front of Farol Island (as discussed below), for all incident wave conditions. This passage, together with the lagoon topography, also controlled the positions of wave vector convergence and interference in the atoll. During high tides, waves converge from the center of the lagoon to the leeward and windward sides of the reef rim, the zone where wave vectors coming from opposite directions converge. At the leeward side, the vector convergence coincides with the reef island locations. In turn, the wave vectors that penetrate into the lagoon through the reef passage converge with incident and refracted waves on the windward side. An interference zone of wave vectors, characterized by the alignment of wave vectors from different directions, is observed behind the windward convergence zone and near the Zulu shingle bank.

The model simulation results for different incident wave conditions (northern and southern swell and southeast wind waves) show small modifications in the wave refraction patterns across the atoll. The wave vector convergence and interference zone positions are very similar during southern swell and southeastern wind wave conditions and slightly dislocated to the south during northern swell conditions. In contrast, differences in the wave power were observed according to incident wave characteristics. The highest wave power values in the lagoon and the reef rim were observed during the northern swell. As shown by the morphology (Fig. 3), the elevation of the leeward reef rim is approximately 2 m lower than that of the windward reef rim. Therefore, offshore waves incoming from the leeward side are less dissipated at the reef edge and can propagate into the lagoon, as well as to Farol Island oceanward beach, with a higher energy. This difference in wave energy is also facilitated by the larger reef passage at the

leeward side. Wind waves incoming from the southeast result in less energetic conditions in the lagoon and at the leeward side. In turn, southern swells result in an intermediate wave power magnitude. These swells are more intensively refracted on the reef rim than wind waves and reach the leeward side with more energy.

3.2.2. Sea-level rise condition (SLR = 1)

The results show an overall increase in wave power across the atoll in the SLR = 1 scenario (Fig. 4b, d, e), with wave power ranging between 0 and 38.5 kW/m. The SLR = 1 scenario also results in changes in the refraction pattern, especially at the windward side of the atoll. The wave vectors do not converge at the center of the lagoon and at the windward side, as is the case for SLR = 0. Instead, a marked interference zone is formed at the windward side, with waves from south and southeast propagating to the leeward side. For northern wave conditions, the lagoon convergence zone is dislocated southward. However, wave vectors still converge on the leeward side due to wave refraction at the reef edge and wave penetration through the reef passage. Nevertheless, this passage imposes less of an influence on wave refraction in the SLR = 1 scenario than in the SLR = 0 scenario. Therefore, the conditions of SLR = 1 allow lagoonward wave propagation to occur with less dissipation, contributing to the wave vector convergence at the leeward side for all incident wave conditions.

3.2.3. Spatial and temporal wave window action

The SLR = 0 scenario was simulated for high, intermediate and low tide conditions to evaluate spatial and temporal wave characteristic variations along a full tidal cycle. The results show that Hs and Tp are strongly modulated by the tide. As the tide drops, the attenuation of Hs and Tp increases (Fig. 5), and the wave action field is restricted to the perennial lagoon (Fig. 6). During low tides, Hs is attenuated by 91%, whereas Tp is attenuated by 75%. At this tidal stage and part of the intermediate tide stage, the sand apron becomes exposed. There is a spatial difference in the magnitude of attenuation between swell and wind waves. Although the period of northern swell waves are higher than the southeastern wind waves at the lagoon, they are more dissipated by the reef rim (75%) and the shallow lagoon (60%) when compared the incident versus transmitted period. Incident wind waves period are nearly homogenous attenuated by the reef rim and the lagoon (53%).

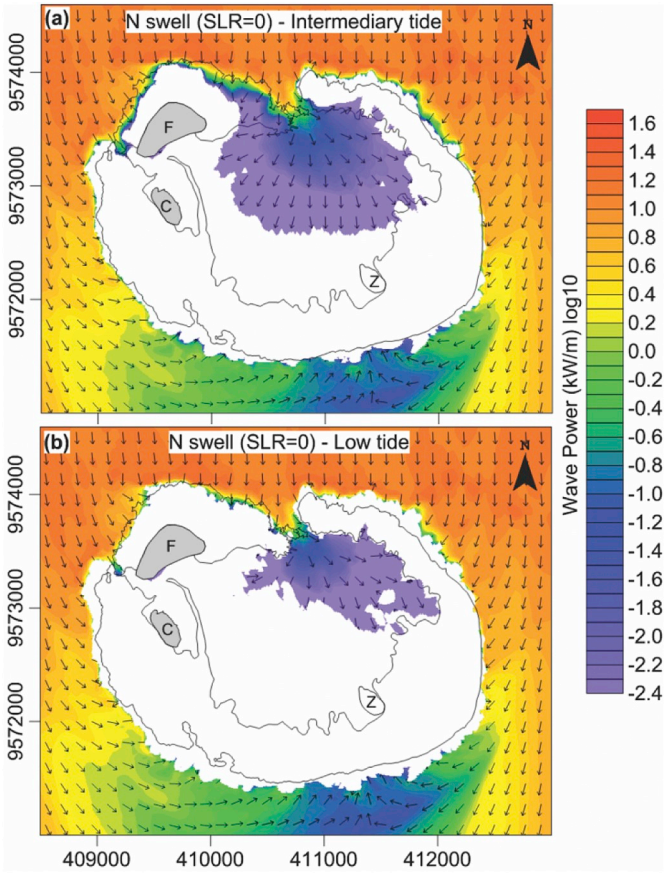

Fig. 6. Spatial wave window action during the (a) intermediate and (b) low tides. Note that wave action is restricted to the perennial lagoon during low tides.

The reef islands are only affected by wave action close to high tide, when the water level reaches their perimeter. This corresponds to a temporal window of 5 h 40 min at each 12 h 25 min semidiurnal interval, which is approximately 46% of a tidal cycle. In the SLR = 1

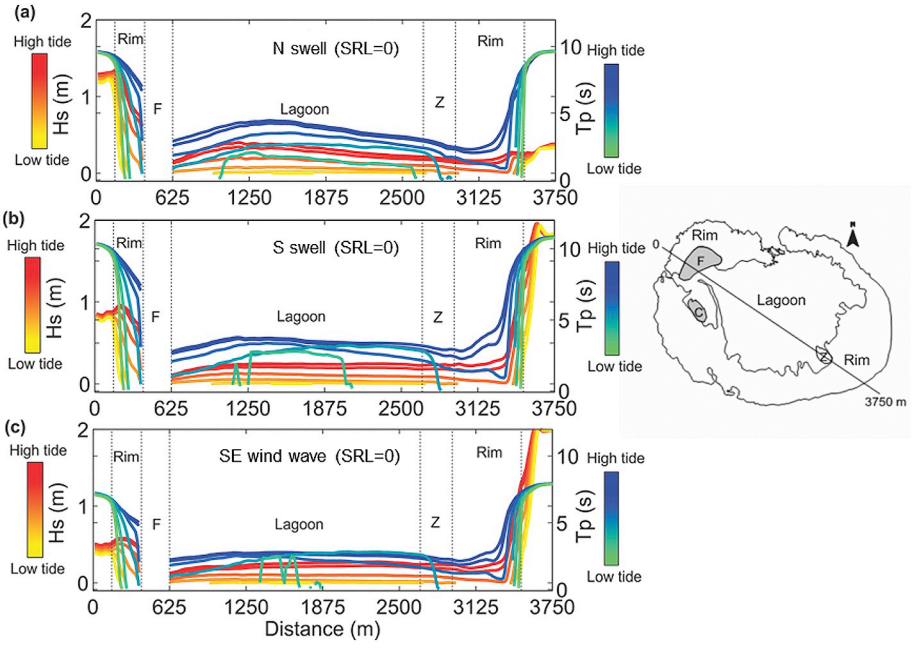

Fig. 5. Cross-profile of significant wave height (Hs) and peak wave period (Tp) from the leeward to windward over a tidal cycle for the SLR = 0 scenario. (a) Northern swell conditions, (b) southern swell conditions and (c) southeastern wind waves. Vertical lines indicate the reef rim (Rim), Farol Island (F), lagoon (Lagoon) and Zulu shingle bank (Z) limits.

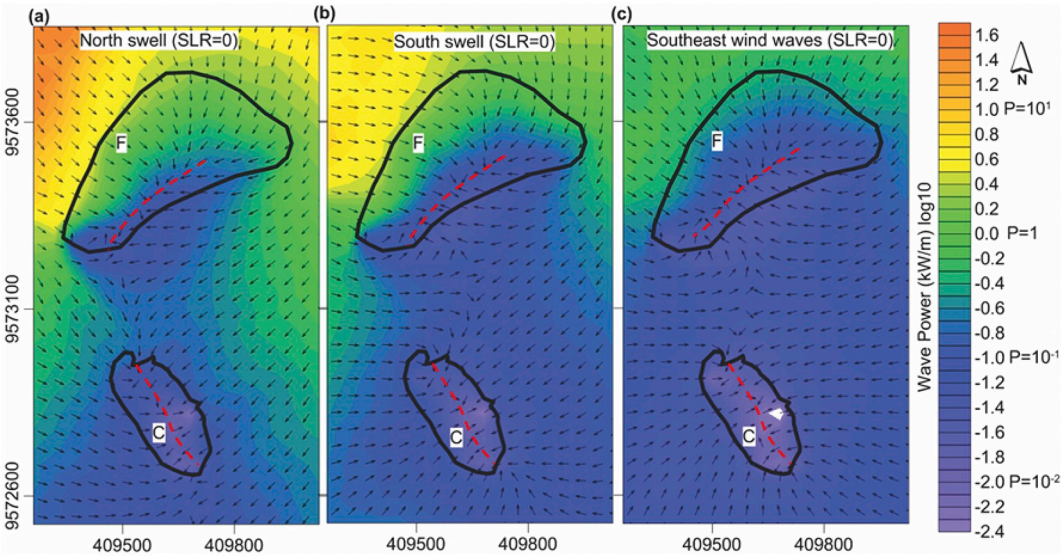

Fig. 7. Details of wave vectors at the reef island locations for SLR = 0 m. Letters on the map correspond to Farol Island (F) and Cemitério Island (C). The wave convergence locations at the reef islands are indicated by red dotted lines. Wave vectors are not scaled. (For interpretation of the references to colour in this figure legend, the reader is referred to the web version of this article.)

scenario, the temporal window of wave action on the reef islands increases to 57% of a tidal cycle.

3.3. Wave vectors convergence

The convergence of wave vectors at the leeward side of the atoll, where the reef islands are located, is shown in detail in Fig. 7 andFigure 8 for SLR = 0 and SLR = 1, respectively. Model simulations show that wave vectors converge at the center of Cemitério Island and near the lagoonward side of Farol Island for SLR = 0 (Fig. 7). The oceanward beach of this island, which is farther from the convergence line, is also subject to more energetic waves than other beaches from both islands, especially during northern swell conditions. Offshore waves from the south and southeast are refracted on the reef rim and reach the oceanward side of Farol Island from the west, reaching the shoreline at approximately 110°. For northern offshore waves, less refraction is observed, and waves reach the oceanward beach with an angle of 70° to the shoreline. In contrast, the lagoonward beach of this island is less exposed to incident energetic waves. The average wave power of this beach is approximately 67% lower than that of the oceanward beach. Waves reach the shoreline almost perpendicularly during offshore southern and southeastern conditions and with an angle of 45° during northern wave conditions. The difference in the magnitudes of Hs and Tp that reach both sides of Farol Island is also shown in Fig. 4. In contrast, beaches at Cemitério Island do not show a significant difference in incident wave energy, except during northern swell conditions, when the lagoonward beach of Cemitério Island receives more wave energy than its oceanward beach.

For all three incident wave conditions in the SLR = 1 scenario, model simulations demonstrate a slight displacement of the wave vector convergence at the Farol Island location and virtually no changes in this convergence at the Cemitério Island location (Fig. 8). The

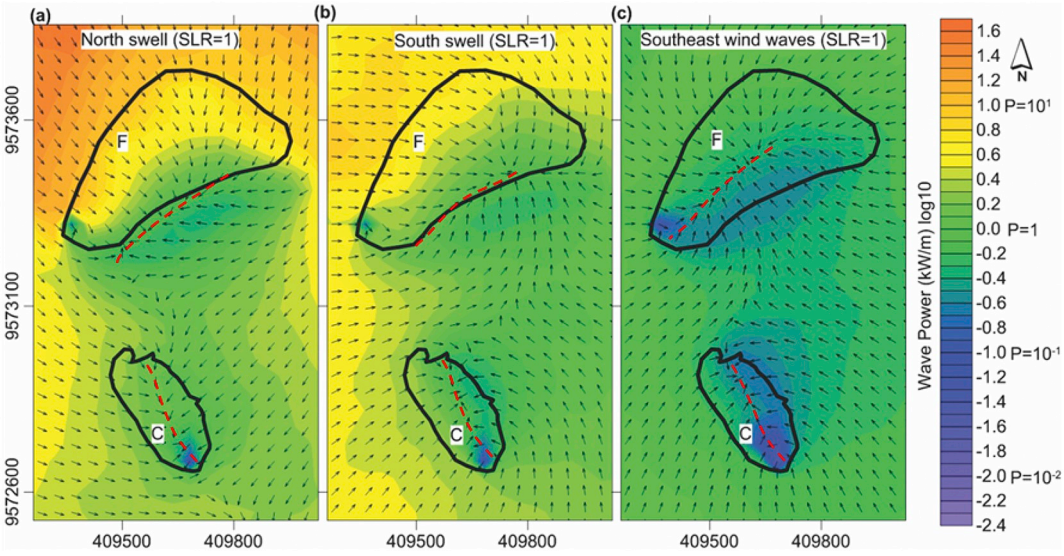

Fig. 8. Details of wave vector convergence at the reef island locations for SLR = 1 m. Letters on the map correspond to Farol Island (F) and Cemitério Island (C). The wave convergence locations at the reef islands are indicated by red dotted lines. Wave vectors are not scaled. (For interpretation of the references to colour in this figure legend, the reader is referred to the web version of this article.)

Table 2
Summary of wave vector convergence locations and displacement in the SLR = 0 and SLR = 1 scenarios for each incident wave condition.

Wave vector convergence position	Wave condition		
	Northern swell	Southern swell	Southeastern wind waves
Scenario 1 (SLR = 0)			
Distance from Oceanward shoreline (m)	220.41	219.81	185.65
Distance from Lagoonward shoreline (m)	35.59	36.19	70.35
Scenario 2 (SLR = 1)			
Distance from Oceanward shoreline (m)	293.44	253.59	157.56
Distance from Lagoonward shoreline (m)	30.54	2.41	98.44
Scenario 1–2			
Displacement (m)	73.03	33.78	−28.09
Displacement direction	Lagoonward	Lagoonward	Oceanward

direction of the displacement is related to the wave period (swell or wind waves) instead of offshore wave direction. The results show that offshore incident swell (from the north or south) induces a vector convergence displacement towards the lagoon, while offshore incident wind waves induce a displacement towards the reef edge. Wave vectors are moved lagoonward by 73 m and 33 m for northern and southern swell wave conditions, respectively. For wind waves, wave vectors are moved 28 m oceanward. Table 2 contains a summary of wave vector locations and displacements in SLR = 0 and SLR = 1 scenarios for each incident wave condition.

The results show an increase in wave power heterogeneity around the reef islands with rising sea level (SLR = 1 scenario). The average wave power reaching the oceanward beach of Farol Island increases 84% for northern swell conditions, 65% for southern swell conditions and 52% for southeastern wind wave conditions. At the lagoonward, in turn, the average wave power has the highest increase for southern swell conditions (79%), followed by southeastern wind wave (69%) and northern swell (24%) conditions. The increase in the lagoonward wave power is thus small compared to the increase in oceanward wave power for northern swell conditions, resulting in a greater displacement of wave vector convergence towards the lagoon.

4. Discussion

4.1. Atoll topography, wave refraction and reef island distribution

Despite being generally defined as mid-ocean annular reefs enclosing a lagoon (Barry et al., 2007), atolls have highly variable sizes and shapes (Shimazaki et al., 2006; Stoddart, 1965), with sizes ranging from > 10,000 km^2 to < 1 km^2 (Costa et al., 2017a). In general, large atolls exhibit very different morphological characteristics than small atolls, and the former are normally composed by deeper lagoons (Wiens, 1962) that can comprise numerous small reef platforms (or table reefs) (Purdy and Winterer, 2001; Woodroffe and Biribo, 2011). Rocas belongs to the small-sized atoll group, with a shallow lagoon and almost continuous reef rim interrupted only by two reef passages. Due to its morphology, the model simulation results (Fig. 4) show that Rocas is similar to an elliptical platform reef (e.g., Gourlay, 1988; Mandlier and Kench, 2012) in terms of wave refraction patterns. Wave vectors converge mainly on the leeward side, and an interference zone can be observed from the windward side through the lagoon. Therefore, as observed for platforms reefs (Gourlay, 1988), the Rocas structure acts both as an obstruction blocking the transmission of wave energy and as a lens for focusing that energy.

However, our numerical results considering a complex bathymetry show that the locations of convergence zones are not only influenced by the wave direction and its interactions with the elliptical reef shape but are also controlled by topographic variations in the reef structure. In particular, the presence of a wide reef passage on the leeward margin has an important role in the wave refraction patterns of Rocas Atoll. For example, for either northern or southern swells, only slight variations in the convergence zones are observed (Figs. 7 and 8). This passage affects the refraction process by allowing offshore waves from different directions to penetrate into the lagoon with less dissipation, thus controlling the location of the convergence zone. This observation was possible via the application of a model that uses the real atoll morphology to simulate wave propagation. Previous studies on such processes have been based on idealized elliptical morphology with a uniform depth and vertical reef faces (e.g., Gourlay, 1988; Mandlier and Kench, 2012; Meijer, 2014).

The distribution of reef islands on Rocas is, in turn, closely related to the wave convergence zone location (Figs. 7 and 8). Such islands are typical sand cays, defined as sedimentary deposits composed mainly of sands (Richmond, 1992) found on lower energy or leeward margins (Stoddart and Steers, 1977). Often, this type of sandy reef island occurs in areas without disturbances such as tropical storms (McLean and Woodroffe, 1997). In areas that experience occasional storms, rubble may exist along the most exposed beaches (Woodroffe, 2008). Consequently, morphological differences have been identified between atolls in storm-prone areas and those closer to the Equator, where tropical cyclones are rare (Woodroffe and Biribo, 2011). Rocas also exhibits a shingle bank on the windward side, as expected for an elliptical platform (Gourlay, 1988; Mandlier and Kench, 2012). According to Gourlay (1988), this type of sedimentary deposit is formed from large pieces of reef material that are broken and displaced from the reef edge during extreme meteorological events, although at Rocas it is predominantly composed of gravel (Pereira et al., 2013). The shingle bank location in Rocas corresponds to a zone of the alignment of wave vectors from different directions and may be formed of material transported from the windward reef rim by occasional energetic swells generated by mid and high-latitude storms (e.g., Smithers and Hoeke, 2014). In turn, consistently unidirectional wave-generated currents can be an important driver in the transport of sediments from other parts of the atoll, such as sand aprons and the windward reef rim, that are subsequently deposited on wave convergences zones at the leeward side of the atoll where the reef islands are located (Costa et al., 2017b).

4.2. Sea-level rise and wave vector convergence displacement

Wave attenuation is highly dependent on water depth over reefs (Costa et al., 2016; Hardy et al., 1991; Kench et al., 2006; Lugo-Fernández et al., 1998). As a consequence, sea-level rise is shown to increase the wave energy able to propagate onto reef flats and lagoons reaching reef-protected shorelines (Baldock et al., 2014; Sheppard et al., 2005; Storlazzi et al., 2015). Although such processes are widely recognized, the effects of sea-level rise on wave refraction over reefs has

received little investigation. Mandlier and Kench (2012) suggested that increases in water depth over reefs cause wave convergence zones to migrate away from the windward reef margin.

Model simulations for Rocas show the displacement of the convergence zone and increases wave energy with sea-level rise (Figs. 7 and 8). However, the direction of this displacement is more sensitive to the incident wave period than the wave direction. Swell waves, either from the north or south, tend to move the convergence zone lagoonwards, whereas wind waves tend to move this zone seawards (Table 2). This pattern can be explained by the larger refraction potential of longer waves in shallow water. In contrast, very short waves may propagate over a platform as intermediate or deep water waves, subsequently limiting or inhibiting the interaction with the submerged structure (Mandlier and Kench, 2012). Therefore, the refraction of swell waves on the elliptical reef rim results in more energy on the leeward margin of the atoll. At the same time, more energy dissipates from swell waves than from wind waves while propagating through the shallow lagoon. In the case of swell incidence, we observe a greater increase in wave energy on the oceanward side than on the lagoonward side of Farol Island under the sea-level rise scenario, which displaces the convergence zone towards the lagoon. Wind waves, in turn, refract less on the reef edge and dissipate less energy while propagating through the lagoon. The increase in wind wave energy reaching Farol Island under the sea-level rise scenario is higher on the lagoonward than on the oceanward side, as illustrated by the model simulations (Figs. 7 and 8). In this case of SRL = 1, the displacement of the convergence zone caused by wind waves is towards the reef edge (seaward) (Fig. 8).

4.3. Implications for reef island morphodynamics

The wave convergence patterns and spatial variations in wave forcing gradients shown here can be related to the morphological changes in reef island atolls. The results presented in Costa et al. (2017a) show substantial accretion on Farol Island and stability on Cemitério Island at a decadal time scale. The wave convergence zones coincide with the island locations, as discussed above. However, there is a difference in the island mobility and in the wave energy at both locations. At the Cemitério Islands, wave vectors show less variability in position for all incident waves and sea level scenarios. Moreover, this island is anchored by beachrocks that protect its beaches from direct wave impacts (Costa et al., 2017a). These two factors can contribute to the morphological stability of Cemitério Island. Conversely, Farol Island shows more complex morphological changes at both seasonal and daily time scales (Costa et al., 2017a). Farol Island has expanded by almost three times its size due to accretion over the last seven decades, changing from an elongated shape to a horseshoe shape with a central depression (Costa et al., 2017a). The lagoonward accretion was followed by oceanward erosion, representing net lagoonward migration. The wave refraction results show that the seaward side of the island is subjected to higher energetic wave conditions and a higher sensitivity to incident wave direction and period (swell or wind wave), which may explain the high morphological variability of Farol Island. Furthermore, for current sea level conditions, wave vectors tend to converge lagoonward of the island, creating favorable depositional conditions at this position.

Despite the morphological differences between most of the Pacific Ocean Atolls and Rocas Atoll, which is rather similar to an elliptical platform reef where wave energy can refract around the platform (e.g. Gourlay, 1998), our results demonstrate that their reef islands share similar shorelines changes and mobility over the last decades. Accretion accompanied by lagoonward migration, such as the pattern observed at Farol Island, has also been described in many Pacific atolls as one of a spectrum of geomorphic changes due to sea-level rise (Webb and Kench, 2010). Webb and Kench (2010) demonstrated that 86% of 27 atoll islands have remained stable or have increased in area during the last several decades. For the same period, sea-level rise around these islands has been estimated at $2\,mm.yr^{-1}$ (Webb and Kench, 2010). Kench et al. (2015), based on 29 studied islands (Funafuti Atoll), observed that the total land area over the past century increased by 7.3%; with more than half of the atoll islands increasing in size in a region where the sea level has been rising $5\,mm.yr^{-1}$. Recently, Duvat et al. (2017) bring more evidences on the persistence of Pacific Ocean reef islands, as 77% of 111 studied islands were stable over the last decades, while 15% and 8% showed an increase or decrease in area, respectively. Estimated absolute sea-level rise in the northern Tuamotu region is about $2.5\,mm.yr^{-1}$ (Becker et al., 2012). Over the few studies that assess multi-decadal planimetric changes on elliptical platform reef, results from Dawnson and Smithers (2010) on Raine Island at the Great Barrier Reef suggest a 6% increase in area at a decadal scale.

With increasing water depth over reefs, larger waves can reach the oceanward shores of reef islands, promoting erosion (Sheppard et al., 2005; Sheppard, 2002; Storlazzi et al., 2015). The aggregated effect of ocean shoreline displacement and lagoon progradation is a shift in the nodal position of islands on reef surfaces (Webb and Kench, 2010). Wave model simulations on Rocas Atoll demonstrated that convergence zone changes due to sea-level rise can promote reef island migration. However, the direction of the shift (towards the lagoon or towards the reef edge) is controlled by the incident wave period (swell or wind wave).

Thus, the results suggest that, under sea-level rise scenarios, areas prone to sediment accumulation will become less stable. The relative frequency between swell and wind wave incidence will be an important driver of morphological change patterns at reef islands. Assuming that the rate of sea-level rise exceeds the potential reef accretion rate (Woodroffe and Webster, 2014) and that the submergence of reefs is accelerated because of climate-driven perturbations (Perry et al., 2018; Perry and Morgan, 2017), it is suggested that the reef island migration observed at Rocas Atoll may be related to a tendency of increasing water depths over the reef surface during the last decades. Reef accretion rates at Rocas Atoll have been estimated to be similar to coral dominated reefs (Gherardi and Bosence, 2005), although Ferreira et al. (2012) showed an increase in water temperature over the last decades, which may lead to stresses that can restrict reef growth and complexity. This implies in a decrease in the wave attenuation capacity by the oceanward reef rim and the displacement of the wave convergence zone lagoonward, as observed by the numerical model results. These results provide important information for the management of reef islands where numerical models can be applied to verify trends in wave convergence and reef island migration.

Acknowledgements

This study was funded by CNPq through the Project “Processos induzidos por ondas e marés no Atol das Rocas: implicações geomorfológicas e projeções futuras” (CNPq 486572/2012-9), by the INCT Ambientes Tropicais Marinhos (CNPq/MCTI) and by FAPESP (Fundação de Apoio a Pesquisa do Estado de São Paulo, Brazil NO.2011/22661-3). We are very grateful to the ICMBio (Instituto Chico Mendes de Conservação da Biodiversidade), especially to Maurizélia Brito, the manager of the marine protected area of Rocas Atoll (REBIO Atol das Rocas), who provided all of the necessary support to our expeditions. Eduardo Siegle was sponsored by a CNPq research fellowship.

References

Allard, J., Bertin, X., Chaumillon, E., Pouget, F., 2008. Sand spit rhythmic development: a potential record of wave climate variations? Arçay Spit, western coast of France. Mar. Geol. 253, 107–131. https://doi.org/10.1016/j.margeo.2008.05.009.

Baldock, T.E., Golshani, A., Callaghan, D.P., Saunders, M.I., Mumby, P.J., 2014. Impact of sea-level rise and coral mortality on the wave dynamics and wave forces on barrier reefs. Mar. Pollut. Bull. 83, 155–164. https://doi.org/10.1016/j.marpolbul.2014.03.058.

Barry, S.J., Cowell, P.J., Woodroffe, C.D., 2007. A morphodynamic model of reef-island development on atolls. Sediment. Geol. 197, 47–63. https://doi.org/10.1016/j.sedgeo.2006.08.006.

Battjes, J.A., Janssen, J.P.F.M., 1978. Energy loss and set-up due to breaking of random waves. In: Proc. 16th Int. Conf. Coastal Eng, pp. 569–587.

BDC, 2015. Banco de Dados Climatológicos do Comando da Aeronáutica—DaEdos para a estação SNFN entre o período de 2006 a 2014. www.icea.gov.br/climatologia/index.html.

Becker, M., Meyssignac, B., Letetrel, C., Llovel, W., Cazenave, A., Delcroix, T., 2012. Sea level variations at tropical Pacific islands since 1950. Glob. Planet. Chang. 80–81, 85–98. https://doi.org/10.1016/j.gloplacha.2011.09.004.

Bellini, C., Marcovaldi, M.A., Sanches, T.M., Grossman, A., Sales, G., 1996. Atol das Rocas Biological Reserve: second largest Chelonia rookery in Brazil. Mar. Turt. Newsl. 1–28.

Booij, N., Ris, R.C., Holthuijsen, L.H., 1999. A third-generation wave model for coastal regions. I- Model description and validation. J. Geophys. Res. 104, 7649–7666. https://doi.org/10.1029/98jc02622.

Church, J.A., Clark, P.U., Cazenave, A., Gregory, J.M., Jevrejeva, S., Levermann, A., Merrifield, M.A., Milne, G.A., Nerem, R., Nunn, P.D., Payne, A.J., Pfeffer, W.T., Stammer, D., Unnikrishnan, A.S., 2013. Sea level change. Clim. Chang. 2013 Phys. Sci. Basis. Contrib. Work. Gr. I to Fifth Assess. Rep. Intergov. Panel Clim. Chang. pp. 1137–1216. https://doi.org/10.1017/CB09781107415315.026.

Costa, M.B.S.F., Araújo, M., Araújo, T.C.M., Siegle, E., 2016. Influence of reef geometry on wave attenuation on a Brazilian coral reef. Geomorphology 253, 318–327. https://doi.org/10.1016/j.geomorph.2015.11.001.

Costa, M.B., Macedo, E.C., Siegle, E., 2017a. Planimetric and volumetric changes of reef islands in response to wave conditions. Earth Surf. Process. Landforms. 42, 2663–2678. https://doi.org/10.1002/esp.4215.

Costa, M.B., Macedo, E.C., Valle-Levinson, A., Siegle, E., 2017b. Wave and tidal flushing in a near-equatorial mesotidal atoll. Coral Reefs 36, 277–291. https://doi.org/10.1007/s00338-016-1525-x.

Dan, S., Walstra, D.-J.R., Stive, M.J.F., Panin, N., 2011. Processes controlling the development of a river mouth spit. Mar. Geol. 280, 116–129. https://doi.org/10.1016/j.margeo.2010.12.005.

Dawson, J.L., Smithers, S.G., 2010. Shoreline and beach volume change between 1967 and 2007 at Raine Island, Great Barrier Reef, Australia. Glob. Planet. Chang. 72, 141–154.

Duvat, V.K.E., Salvat, B., Salmon, C., 2017. Drivers of shoreline change in atoll reef islands of the Tuamotu Archipelago. French Polynesia. Glob. Planet. Change 158, 134–154. https://doi.org/10.1016/j.gloplacha.2017.09.016.

Ferreira, B.P., Costa, M.B.S.F., Coxey, M.S., Gaspar, A.L.B., Veleda, D., Araujo, M., 2012. The effects of sea surface temperature anomalies on oceanic coral reef systems in the southwestern tropical Atlantic. Coral Reefs 32, 441–454.

Filipot, J.-F., Cheung, K.F., 2012. Spectral wave modeling in fringing reef environments. Coast. Eng. 67, 67–79. https://doi.org/10.1016/j.coastaleng.2012.04.005.

Flood, P.G., 1986. Sensitivity of coral cays to climatic variations, southern Great Barrier Reef, Australia. Coral Reefs 5, 13–18. https://doi.org/10.1007/BF00302166.

Forbes, D.L., James, T.S., Sutherland, M., Nichols, S.E., 2013. Physical basis of coastal adaptation on tropical small islands. Sustain. Sci. 8, 327–344. https://doi.org/10.1007/s11625-013-0218-4.

Gherardi, D.F.M., Bosence, D.W.J., 2005. Late Holocene reef growth and relative sea level changes in Atol das Rocas, equatorial South Atlantic. Coral Reefs 24, 264–272. https://doi.org/10.1007/s00338-005-0475-5.

Godley, B.J., Saunders, K.E., Hartnoll, R.G., Broderick, A.C., 2009. Population Structure of the Land Crab Johngarthia Lagostoma on Ascension Island. J. Crustac. Biol. 29, 57–61. https://doi.org/10.1651/08-2992.1.

Golshani, A., Baldock, T.E., Mumby, P.J., Callaghan, D.P., Nielsen, P., Phinn, S., 2012. Climate impacts on hydrodynamics and sediment dynamics at reef islands. In: Proc 12th Int Coral Reef Sym, Cairns, Australia, pp. 10–13.

Gourlay, M.R., 1988. Coral cays: products of wave action and geological processes in a biogenic environment. Proc. 6th Int. Coral Reef Symp. 2, 6–11.

Hardy, T., Young, I.R., Nelson, R.C., Gourlay, M., 1991. Wave Attenuation on an Offshore Coral Reef. Proc. 22nd Coast. Energy Conf. I. pp. 330–344.

Hoeke, R.K., 2010. An Investigation of Wave- Dominated Coral Reef Hydrodynamics. James Cook University.

Hoeke, R.K., Storlazzi, C.D., Ridd, P.V., 2013. Drivers of circulation in a fringing coral reef embayment: a wave-flow coupled numerical modeling study of Hanalei Bay, Hawaii. Cont. Shelf Res. 58, 79–95. https://doi.org/10.1016/j.csr.2013.03.007.

Hoeke, R.K., Storlazzi, C., Ridd, P., 2011. Hydrodynamics of a bathymetrically complex fringing coral reef embayment: Wave climate, in situ observations, and wave prediction. J. Geophys. Res. 116, C04018. https://doi.org/10.1029/2010JC006170.

Holthuijsen, L.H., Booij, N., Herbers, T.H.C., 1989. A Prediction Model for Stationary, Short-crested Waves in Shallow Water with Ambient Currents. Coast. Eng. 13, 23–54.

Kench, P.S., Brander, R.W., 2006. Response of reef island shorelines to seasonal climate oscillations: south Maalhosmadulu atoll. Maldives. J. Geophys. Res. 111, F01001. https://doi.org/10.1029/2005JF000323.

Kench, P.S., Brander, R.W., Parnell, K.E., McLean, R.F., 2006. Wave energy gradients across a Maldivian atoll: Implications for island geomorphology. Geomorphology 81, 1–17. https://doi.org/10.1016/j.geomorph.2006.03.003.

Kench, P.S., Brander, R.W.W., Parnell, K.E.E., O'Callaghan, J.M.M., 2009a. Seasonal variations in wave characteristics around a coral reef island, South Maalhosmadulu atoll, Maldives. Mar. Geol. 262, 116–129. https://doi.org/10.1016/j.margeo.2009.03.018.

Kench, P.S., Parnell, K.E., Brander, R.W., 2009b. Monsoonally influenced circulation around coral reef islands and seasonal dynamics of reef island shorelines. Mar. Geol. 266, 91–108. https://doi.org/10.1016/j.margeo.2009.07.013.

Kench, P.S., Thompson, D., Ford, M.R., Ogawa, H., McLean, R.F., 2015. Coral islands defy sea-level rise over the past century: Records from a central Pacific atoll. Geology 43, 515. https://doi.org/10.1130/g36555.1.

Lowe, R.J., Hart, C., Pattiaratchi, C.B., 2010. Morphological constraints to wave-driven circulation in coastal reef-lagoon systems: a numerical study. J. Geophys. Res. 115, C09021. https://doi.org/10.1029/2009JC005753.

Lugo-Fernández, A., Roberts, H.H., Wiseman, W.J., 1998. Tide effects on wave attenuation and wave set-up on a Caribbean coral reef. Estuar. Coast. Shelf Sci. 47, 385–393.

Madsen, O., Poon, Y., Graber, H., 1988. Spectral wave attenuation by bottom friction: theory. In: Coastal Engineering. ASCE, pp. 492–504. https://doi.org/10.9753/icce.v21.

Mandlier, P.G., 2013. Field observations of wave refraction and propagation pathways on coral reef platforms. Earth Surf. Process. Landforms 38, 913–925. https://doi.org/10.1002/esp.3328.

Mandlier, P.G., Kench, P.S., 2012. Analytical modelling of wave refraction and convergence on coral reef platforms: implications for island formation and stability. Geomorphology 159–160, 84–92. https://doi.org/10.1016/j.geomorph.2012.03.007.

McGregor, G.R., Nieuwolt, S., 1998. Tropical climatology — An introduction to the climates of the low latitudes, 2nd ed. John Wiley and Sons, New York. https://doi:978-0-471-96611-1.

McKoy, H., Kennedy, D.M., Kench, P.S., 2010. Sand cay evolution on reef platforms, Mamanuca Islands. Fiji. Mar. Geol. 269, 61–73. https://doi.org/10.1016/j.margeo.2009.12.006.

McLean, R.F., Woodroffe, C.D., 1997. Coral atolls. In: Carter, R.W.G., Woodroffe, C.D. (Eds.), Coastal Evolution: Late Quaternary Shoreline Morphodynamics. Cambridge University Press, Cambridge, UK, pp. 267–302.

Meijer, J.J., 2014. Modelling the Formation of Coral Cays on Platform Reefs. Utrecht University. Thesis, pp. 64.

Pattiaratchi, C., Olsson, D., Hetzel, Y., Lowe, R., 2009. Wave-driven circulation patterns in the lee of groynes. Cont. Shelf Res. 29, 1961–1974. https://doi.org/10.1016/j.csr.2009.04.011.

Pereira, N.S., Manso, V.V., Macedo, R.J., Dias, J.M.A., Silva, A.M.C., 2013. Detrital carbonate sedimentation of the Rocas Atoll, South Atlantic. An. Acad. Bras. Cienc. 85, 52–72. https://doi.org/10.1590/S0001-37652013000100005.

Perry, C.T., Morgan, K.M., 2017. Bleaching drives collapse in reef carbonate budgets and reef growth potential on southern Maldives reefs. Sci. Rep. 7, 1–9. https://doi.org/10.1038/.

Perry, C.T., Alvarez-Filip, L., Graham, N.A.J., Mumby, P.J., Wilson, S.K., Kench, P.S., Derek, P., 2018. Loss of coral reef growth capacity to track future increases in sea-level. Nature. https://doi.org/10.1038/s41586-018-0194-z.

Purdy, E.G., Winterer, E.L., 2001. Origin of atoll lagoons. Bull. Geol. Soc. Am. 113, 837–854. https://doi.org/10.1130/0016-7606(2001)113<0837:OOAL>2.0.CO;2.

Richmond, B.M., 1992. Development of Atoll Islets in the Central Pacific. In: Proceedings of the Seventh International Coral Reef Symposium. Guam, pp. 1185–1194.

Sato, D., Yokoki, H., 2010. Numerical calculation on shoreline conservation in Majuro atoll, the Marshall Islands. In: Proceedings of the Coastal Engineering Conference. Shangai, pp. 1–14.

Schulz-Neto, A., 2004. Aves Marinhas do Atol das Rocas. In: Branco, Joaquim Olinto (Ed.), Aves Marinhas e Insulares Brasileiras: Bioecologia e Conservação. UNIVALI, Itajaí, SC, pp. 169–192.

Sheppard, C.R.C., 2002. Island elevations, reef condition and sea level rise in atolls of Chagos. In: British Indian Ocean Territory, Coral Reef Degradation in the Indian Ocean. Status Report 2002. Kalmar, Sweden.

Sheppard, C., Dixon, D.J., Gourlay, M., Sheppard, A., Payet, R., 2005. Coral mortality increases wave energy reaching shores protected by reef flats: examples from the Seychelles. Estuar. Coast. Shelf Sci. 64, 223–234. https://doi.org/10.1016/j.ecss.2005.02.016.

Shimazaki, H., Yamano, H., Yokoki, H., Yamaguchi, T., Chikamori, M., Tamura, M., Kayanne, H., 2006. Global mapping of factors controlling reef-island formation and maintenance. In: Proceedings of 10th International Coral Reef Symposium, pp. 1577–1584.

Siegle, E., Costa, M.B., 2017. Nearshore wave power increase on reef shaped coasts due to sea-level rise. Earth's Futur. 5, 1054–1065. https://doi.org/10.1002/2017EF000624.

Smithers, S.G., Hoeke, R.K., 2014. Geomorphological impacts of high- latitude storm-waves on low-latitude reef islands: observations of the December 2008 event on Nukutoa, Takuu, Papua New Guinea. Geomorphology 222, 106–121.

Sorensen, O.R., Kofoed-Hansen, H., Rugbjerg, M., Sorensen, L.S., 2004. A third-generation spectral wave model using an unstructured finite volume technique. In: Proceedings of the 29th Intern. Conf. on Coastal Eng, pp. 894–906.

Stoddart, D.R., 1965. The shape of atolls. Mar. Geol. 3, 369–383.

Stoddart, D.R., Steers, J.A., 1977. The nature and origin of coral reef islands. In: Jones, A.O., Endean, R. (Eds.), Biology and Geology of Coral Reefs. Geology 2, vol. IV. Academic Press, New York, pp. 59–105.

Stone, G.W., Zhangf, X., Sheremetfij, A., 2005. The role of barrier islands , muddy shelf and reefs in mitigating the wave field along Coastal Louisiana. J. Coast. Res. 44, 40–50.

Storlazzi, C.D., Elias, E., Field, M.E., Presto, M.K., 2011. Numerical modeling of the

impact of sea-level rise on fringing coral reef hydrodynamics and sediment transport. Coral Reefs 30, 83–96. https://doi.org/10.1007/s00338-011-0723-9.
Storlazzi, C.D., Elias, E.P.L., Berkowitz, P., 2015. Many atolls may be uninhabitable within decades due to climate change. Sci. Rep. 5, 14546. https://doi.org/10.1038/srep14546.
Vitousek, S., Fletcher, C., Merrifield, M., Pawlak, G., Storlazzi, C., 2007. Model scenarios of shoreline change at Kaanapali Beach, Maui, Hawaii: seasonal and extreme events. In: Coastal Sediments 07, pp. 1227–1240. https://doi.org/10.1061/40926(239)95.
Webb, A.P., Kench, P.S., 2010. The dynamic response of reef islands to sea-level rise: evidence from multi-decadal analysis of island change in the Central Pacific. Glob. Planet. Change 72, 234–246. https://doi.org/10.1016/j.gloplacha.2010.05.003.
Wiens, H.J.W., 1962. Atoll Environment and Ecology. 22. Yale University Press, New Haven, Connecticut, pp. 532.
Woodroffe, C.D., 2008. Reef-island topography and the vulnerability of atolls to sea-level rise. Glob. Planet. Change 62, 77–96. https://doi.org/10.1016/j.gloplacha.2007.11.001.
Woodroffe, C.D., Biribo, N., 2011. Atolls. In: Hopley, D. (Ed.), Encyclopedia of Modern Coral Reefs: Structure. Form and Process. Springer, The Netherlands, pp. 51–71.
Woodroffe, C.D., Webster, J.M., 2014. Coral reefs and sea-level change. Mar. Geol. 352, 248–267. https://doi.org/10.1016/j.margeo.2013.12.006.